THE JOURNAL OF PHYSICAL CHEMISTRY B

Article

pubs.acs.org/JPCB

Comparison of Binding Ability and Location of Two Mesoporphyrin Derivatives in Liposomes Explored with Conventional and Site-Selective Fluorescence Spectroscopy

Dániel Veres, Barnabás Bőcskei-Antal, István Voszka, Károly Módos, Gabriella Csík, András D. Kaposi, Judit Fidy, and Levente Herenyi*

Department of Biophysics and Radiation Biology, Semmelweis University, POB. 263, H-1444 Budapest, Hungary

ABSTRACT: Application of porphyrins as photosensitizers is based on their light-triggered generation of reactive oxygen species (ROS) that may cause oxidative tissue damage and ultimately kill cells. Cellular membranes are the action grounds of many sensitizers due to their hydrophobic or amphiphilic character as well as the location of many of the targets attacked by ROS. Hence, the binding ability and location of porphyrins in liposomes as simple models of cellular membranes are of outstanding interest. Here we compare mesoporphyrin IX dimethyl ester (MPE) and its nonesterified form, mesoporphyrin IX dihydrochloride (MPCl). Monocomponent small unilamellar vesicles formed of various saturated phosphatidylcholines with incorporated mesoporphyrins were investigated. We determined the binding parameters and the inhomogeneous distribution functions (IDFs) by different fluorescence techniques. We found in general that the binding ability of MPE is considerably greater than that of MPCl. In the case of MPCl, the IDFs suggest that only one of the two binding site types identified earlier for MPE ("site II") exists; the other one ("site I") vanishes while a new one appears ("site III"). We can confirm that "site I" is located between the two lipid layers, "site II" is situated between the hydrocarbon chains, while the location of the novel "site III" is along the outer part of the hydrocarbon chains partially inserted between the lipid head groups.

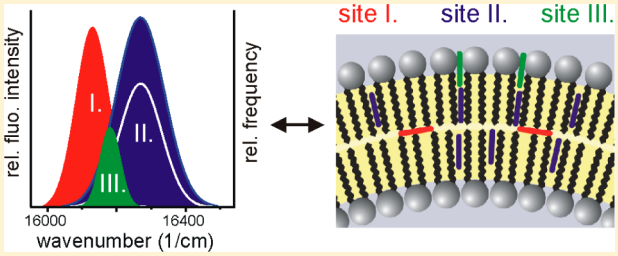

INTRODUCTION

The phenomenon of photosensitization has been known for more than a hundred years. However, it has been rediscovered only recently because of its potential therapeutic applications. One of the most important clinical applications of porphyrinoid sensitizers is photodynamic therapy (PDT). PDT has been developed as a cell killing method; therefore, it has been applied mostly for tumor therapy, but some of the most successful PDT applications are related to nontumorous diseases. PDT involves a nontoxic dye, the photosensitizer (PS), which is excited by visible light and arrives at a triplet state via nonradiant transitions. In this state, the PS interacts with cellular oxygen to form toxic reactive oxygen species (ROS), leading to cell death. In addition, the characteristic fluorescence of PS is also used in diagnostics to determine the location of neoplastic tissues. Photodynamic methods have also been considered for the inactivation of viruses and killing of other microorganisms.[1−7]

The most important factor governing the outcome of the photodynamic effect is the way the PS interacts with cells in the target tissue. One of the main steps in the process is the generation of singlet oxygen. Due to its short lifetime and diffusion pathway, the primary reaction occurs mainly in the close vicinity of the PS molecules.[8,9] Thus, the key aspect of this interaction is the binding ability and the subcellular location of the PS. The favorable pattern of location depends on the nature of the sensitizer as well as on the complex environmental conditions.[10]

Most of the sensitizers used in photodynamic methods are porphyrin derivatives. Because of their hydrophobic or amphiphilic character, they bind to various cellular lipid membranes.[11] Hence, the investigation of the binding of porphyrin derivatives to the membrane and their distribution between the membrane compartments is particularly important. On the basis of this information, one can predict the effectiveness of a photodynamic reaction and decide whether a sensitizer can be considered a good candidate for photodynamic applications.

Many conclusions presented in this field are based on data obtained from membrane model systems such as liposomes, which can mimic specific cellular environments. Noncovalent interactions of the sensitizer with surrounding molecules in liposomes have been explored.[12−14] Numerous articles report on the location of porphyrin molecules and on the nature of interactions based on different fluorescence experimental techniques. The location along the hydrocarbon chains of the PSs in the bilayer has also been studied, and a direct correlation between location depth and photosensitizing activity was demonstrated.[15−18]

Received: May 15, 2012
Revised: July 6, 2012
Published: July 9, 2012

We have previously shown that the location of porphyrin molecules within the lipid bilayer can be determined with great accuracy by site-selective fluorescence spectroscopy.[19] In conventional spectra, beside temperature-induced homogeneous broadening, slight fluctuations of the surrounding matrix lead to inhomogeneity in the chromophore environment and cause inhomogeneous broadening of the spectral bands. Site-selective fluorescence spectroscopy (more precisely, fluorescence line narrowing or FLN spectroscopy) is a high-resolution method capable of monitoring environmental effects free of inhomogeneous broadening. This low temperature technique was reviewed.[20−22] However, since this method is not used frequently, a short summary including our novel concept is given in Appendix I.

In the present work, we applied this technique to compare several systems composed of photosensitizers and lipid membranes. We studied the binding of two mesoporphyrin (MP) derivatives, namely, mesoporphyrin IX dimethyl ester (MPE) and mesoporphyrin IX dihydrochloride (MPCl), to monocomponent small unilamellar vesicles (SUVs) formed of three kinds of saturated phospholipids, namely, dimyristoyl-, dipalmitoyl-, and distearoyl-phosphatidylcholine (DMPC, DPPC, DSPC). By using different phosphatidylcholines, a single parameter, the length of hydrocarbon chains (14, 16, 18 carbon atoms for each, respectively), is varied in the structure of SUVs. The quality of liposome samples was checked by dynamic light scattering (DLS) measurements after each step of both the preparation and the experiment. We demonstrate that the inhomogeneous distribution functions (IDFs) of the two MP derivatives in different liposome environments characterize the location of these molecules, and a structural model of binding sites is introduced on the basis of these functions. Parameters of the binding ability of MPs to various SUVs were determined by conventional fluorescence spectroscopy using a new and accurate evaluation method. We show that this method is suitable to demonstrate the existence of non-equivalent binding sites. We found correlation between the binding ability and the location of MP molecules. Finally, we conclude that high affinity binding sites appear between the SUV lipid layers as a result of esterification of MP, which is an advantageous property with respect to photodynamic applications.

EXPERIMENTAL METHODS

MP-Liposome Sample Preparation. Samples were prepared according to methods described earlier.[19] Stock solutions of mesoporphyrin IX-dimethyl ester (MPE) and mesoporphyrin IX dihydrochloride (MPCl) (both from Frontier Scientific, Inc., Logan, UT) were prepared in dimethyl-formamide (DMF) (Sigma, St. Louis, MO) with a concentration of around 2 mM and kept in a dark place to avoid photodegradation.

Dimyristoyl-, dipalmitoyl-, and distearoyl-phosphatidylcholine (DMPC, DPPC, DSPC) (Sigma, St. Louis, MO) were dissolved in chloroform and then dried with a stream of nitrogen followed by placing in vacuum (≈2 Pa) for 15 min. Samples were kept in a desiccator at least overnight. Lipids were hydrated with phosphate buffered saline (PBS) (10 mM phosphate, 137 mM NaCl, pH 7.4) at a temperature just above the main (liquid−gel) transition temperature (T_m) of the corresponding lipid membrane (≈24, 42, and 55 °C for DMPC, DPPC, and DSPC, respectively). The samples were sonicated for 10 min twice (MSE Soniprep 150 Ultrasonic Disintegrator, frequency 23 kHz; wave-amplitude 8 μm) with a 5 min pause to avoid overheating. Remnants of multilamellar vesicles and contaminants (e.g., Ti particles from the sonicator) were removed by centrifugation (Beckman J2-21 centrifuge, 15000 rpm, 10 min). The final phospholipid concentration was approximately 15 mM. Porphyrin was added to liposome at room temperature (RT ≈ 22 °C).

Samples for Binding Measurements. A series of MP−liposome samples of constant mesoporphyrin [MP] (and DMF) but varying lipid concentrations [L] was prepared by mixing for half an hour. On the basis of the spectroscopic check, we found that binding equilibrium was established by the end of this time.

Samples for Site-Selective Measurements. Porphyrin from stock was added to the liposome in excess and mixed for 2 h. Then, glycerol was added for cryoprotection and to ensure sample transparency at low temperatures (final concentration: 50% (v/v)). The final concentration of the samples was approximately 20 μM and 7 mM for MP and phospholipids, respectively. Spectroscopic measurements were carried out immediately after sample preparation at cryogenic temperature. Remnants of free MP did not disturb the fluorescence measurements because of the significant spectral separation from the emission maximum of associated MP.

Following each step of the sample preparation, the size distribution of liposomes was measured by dynamic light scattering (DLS). Thus, the homogeneity and the possible disintegration or aggregation of the liposome samples were checked.

The different protonation states of MPs at various pH's were analyzed using routines from the Marvin Beans software (ChemAxon Ltd.).

Dynamic Light Scattering (DLS). DLS measurements were performed with equipment consisting of a goniometer system (ALV GmbH, Langen, Germany), a diode-pumped solid-state (DPSS) laser light source (Melles Griot 58-BLS-301, 457 nm, 150 mW), and a light detector (Hamamatsu H7155 PMT module). The evaluation software yielded the autocorrelation function of scattered light intensity, which was further analyzed by the maximum entropy method (MEM)[23,24] from where the different contributions of this function were determined. For spherical particles, this contribution is proportional to the weight of the particle. In the case of unilamellar vesicles, this proportionality holds for r^2 with good approximation where r is the radius of the vesicle. With r^{-2} used as a weighting factor, the particle size distributions were determined.

Fluorescence Spectroscopy. Fluorescence emission spectra were measured with a Fluorolog-3 (model FL3-22) (Jobin Yvon S.A. HORIBA, Longjumeau, France) with double monochromators on both the excitation and the emission side equipped with Xe lamp (450 W) excitation and photomultiplier detection in photon counting mode (Hamamatsu R928P).

Conventional Technique. Samples were kept in a temperature-controlled sample holder at 22 °C, and they were excited at the maximum of the Soret-band (397 nm). Fluorescence emission spectra were recorded by scanning the 600−640 nm range in 0.5 nm steps.

Site-Selective Technique. All measurements were carried out at 10 ± 1 K using a temperature-controlled closed-cycle helium cryostat (Cryophysics, Geneva, Switzerland). Series of fluorescence emission spectra were recorded with the same

dx.doi.org/10.1021/jp304712n | J. Phys. Chem. B 2012, 116, 9644−9652

emission side parameters as above, while the excitation wavelength was varied in 1 nm steps in the 555−585 nm range of the Q region. After the wavelength−frequency conversion, the peaks were fitted by Gaussians. Finally, each peak was characterized by two "changing" parameters: the center of the peak (typical frequency ν_n) and the total area under the peak (proportional to the total emission intensity I_n); the width of the peak was kept constant. From these data, the inhomogeneous distribution function (IDF) was determined (see the Results section).

Determination of Binding Parameters. The association of MP molecules to lipid membranes can be monitored by spectroscopic titration: lipid concentration is varied at constant dye concentration to obtain a calibration of the optical change at infinite lipid concentration when all the dye is bound. In our case, the fluorescence intensity of bound MP molecules (I) was measured as a function of the concentration of the added lipid ([L]). Since we wanted to avoid some evaluation errors,[25,26] instead of the usually applied approaching formula, we turned to the classical equilibrium mass action equation:

$$n[\mathrm{L}]_f[\mathrm{MP}]_f = K_d[\mathrm{MP}]_b \quad (1)$$

where n is the number of the possible binding sites per lipid molecule, $[\mathrm{L}]_f$ is the concentration of free lipid, $[\mathrm{MP}]_f$ and $[\mathrm{MP}]_b$ are the concentrations of MP molecules in free and bound state, respectively, and K_d is the dissociation constant. Equation 1 can be rearranged to express the concentration of bound mesoporphyrin $[\mathrm{MP}]_b$, as an explicit function of the two independent variables, the lipid [L] and the total mesoporphyrin concentration [MP]:

$$[\mathrm{MP}]_b = \frac{1}{2}(n[\mathrm{L}] + [\mathrm{MP}] + K_d - \sqrt{(n[\mathrm{L}] + [\mathrm{MP}] + K_d)^2 - 4n[\mathrm{L}][\mathrm{MP}]}) \quad (2)$$

from where the binding parameters can be determined due to the linear relation between the fluorescence intensity and the concentration of bound fluorochrome. The binding constant as a binding parameter was defined by the equation: $K_b = n/K_d$.

Spectra, IDFs, and binding curves were analyzed using the "nonlinear curve fit" routines of the Origin 7 software (OriginLab Corporation).

RESULTS

Figure 1 shows the normalized conventional fluorescence emission spectra of the two MPs at different conditions. First, we have to pay attention to a remarkable difference: while the spectrum of free MPCl is well measurable (shown in gray), the fluorescence signal of free MPE is undetectable under these circumstances. The other curves are the spectra of MPs completely associated with various SUV samples. A red shift is observable for both MPE and MPCl with decreasing hydrocarbon chain lengths, though to different extents.

Characterization of Binding Ability. *MPE.* Spectroscopic titration was executed for all three SUV samples. Figure 2 shows the MPE-DMPC titration (the other two are not shown). Since the free MPE is nonfluorescent, we could consider the measured fluorescence intensity I as proportional to the $[\mathrm{MP}]_b$. On the basis of these data, a binding curve can be created, but we may get more information from these measurements if we apply a novel evaluation method, which is presented in Appendix II.

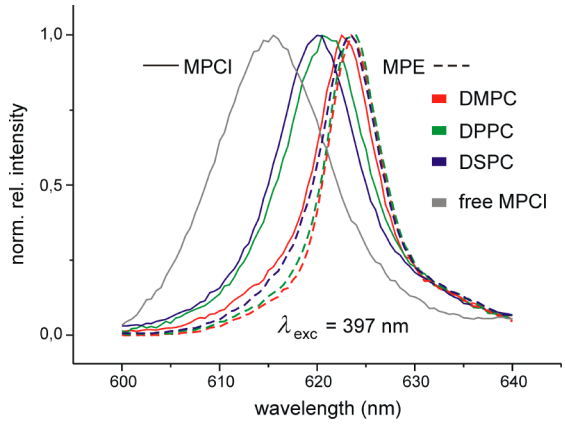

Figure 1. Normalized conventional fluorescence emission spectra of MPE (broken line) and MPCl (solid line) completely associated with different SUV samples in PBS solution at room temperature (RT ≈ 22 °C) excited at 397 nm. The SUVs are composed of either DMPC (red), DPPC (green), or DSPC (blue). The spectrum of free MPCl is shown in gray; the fluorescence signal of free MPE is undetectable under these circumstances.

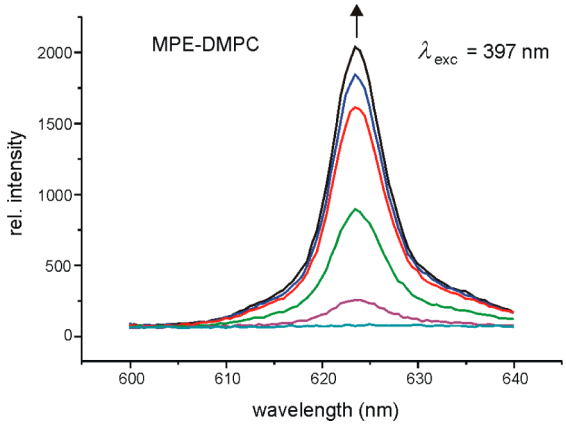

Figure 2. MPE-DMPC titration curve: a series of conventional fluorescence emission spectra at constant MP and varying lipid concentrations (marked with different colors) at room temperature (RT ≈ 22 °C) excited at 397 nm. The arrow shows the effect of MPE binding.

First, we generated the $I_{[L]max}(\lambda) \rightarrow I_{[L]}(\lambda)$ functions (see eq App7) at different lipid concentrations [L] from the titration series. Figure 3 shows three of these linear functions for all the SUV samples at a specific lipid concentration [L]*. In the case of DSPC, the data points form a loop instead of a linear function with random errors. The reason is clear: the two types of binding sites presented earlier[19] are not completely equivalent with respect to the association process. A similar but weaker effect is also present in the case of DPPC but practically nonexistent for DMPC. These results cannot be read directly from the binding curves (see Figure 4) but only from this novel representation.

The MPE-DMPC binding curve can be seen in Figure 4. First, we determined the slopes $k_{[L]}$ of the respective $I_{[L]max}(\lambda) \rightarrow I_{[L]}(\lambda)$ functions by linear fit according to eq App7, and represented them as a function of lipid concentration [L] → $k_{[L]}$. Then, eq 2 was applied as a fitting function, but instead of the concentration of bound mesoporphyrin $[\mathrm{MP}]_b$, we used the respective $k_{[L]}$ values. After the fitting procedure, instead of [MP], we got k_∞ as a fit parameter, which is the estimated slope

dx.doi.org/10.1021/jp304712n | J. Phys. Chem. B 2012, 116, 9644−9652

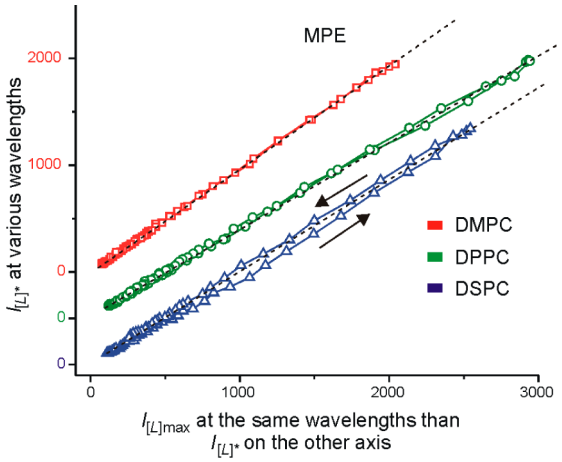

Figure 3. $I_{[L]max}(\lambda) \rightarrow I_{[L]^*}(\lambda)$ functions at a specific lipid concentration (just for demonstration $[L]^* \approx 65 \pm 5\ \mu M$) of MPE in various SUV samples: DMPC (red), DPPC (green), and DSPC (blue) (origin is shifted along the vertical axis; broken lines show the linear fit). In the case of DSPC, a loop is clearly visible because of the hysteresis marked with arrows. The slope $k_{[L]^*}$ of the fitted straight lines gives the relative $[MP]_b$ of the associated MPE in the SUV (see text). (The derivation of this type of representation is seen in Figure 8.)

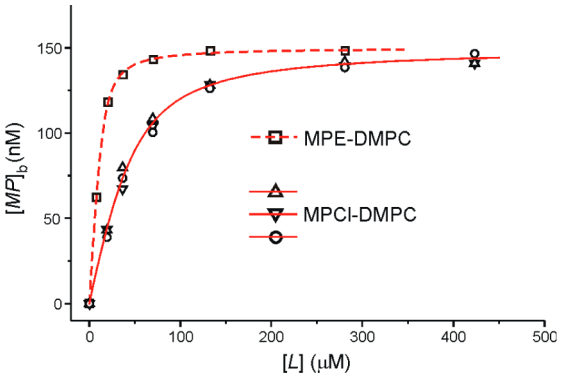

Figure 4. Binding curves of MPE (□; fitting with broken line) and MPCl (△, ▽, ○; fitting with solid line) to DMPC: the concentration of associated porphyrin $[MP]_b$ determined from relative fluorescence intensities as a function of lipid concentration [L]. Different symbols mean different evaluation methods (see text). (Standard errors are comparable to the symbol size.)

at complete binding. Since the measured [MP] was known, we could rescale the vertical axis according to the calculated $[MP]_b$ and the other two unknown parameters, n and K_d, could be obtained by a final fit.

MPCl. Characterization of MPCl binding is more complicated because of the overlapping spectra of free and bound states (see Figure 1).

Figure 5A shows the process of spectroscopic titration of MPCL-DMPC. We applied two methods for getting the binding curves. The first was done by decomposition of spectra using Gaussians, as can be seen in Figure 5B. Area under an increasing band as a fit parameter is proportional to $[MP]_b$. We used both increasing bands marked with open (up and down) triangles, and the final fit results are represented in Figure 4 with the same symbols.

In the case of the other method, we used eq App7 in a modified form:

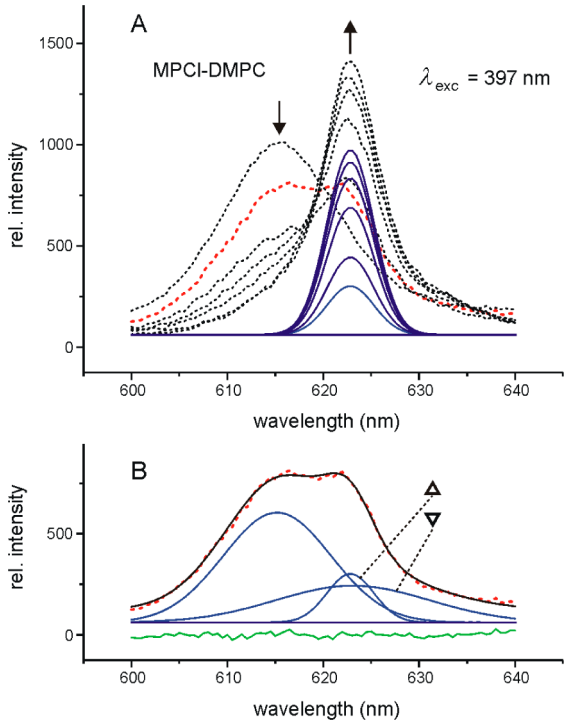

Figure 5. (A) MPCl-DMPC titration curve: a series of conventional fluorescence emission spectra at constant MP and various lipid concentrations (dotted lines), at room temperature (RT ≈ 22 °C), excited at 397 nm. Arrows show the effect of MPCl binding. The leftmost curve is the spectrum of the free MPCl. All the other spectra were decomposed by 3 Gaussians with constant centers and widths. The change of the dominant increasing component is seen as a series of solid blue lines. The areas under these curves are proportional to the concentration of associated MPCl in SUV. (B) An example for the decomposition (red curve in part A): the sum of the three blue components is the black curve, and the green is the residue.

$$(I_{[L]}(\lambda) - C) - q(I_{free}(\lambda) - C) = k_{[L]}I_{[L]max}(\lambda) \quad (3)$$

where q is a weighting factor ($0 \le q \le 1$) and $I_{free}(\lambda)$ is the original spectrum of free MPCl. C and q were varied until the highest correlation coefficient was reached and the slope $k_{[L]}$ could be determined. Further steps of the method are the same as described above for MPE. Data points for the binding curve obtained by this method are also observable in Figure 4 marked with open circles, and all three data series are well fitted by the same red solid line. Binding parameters of both MPs are summarized in Table 1.

Determination of the Inhomogeneous Distribution Functions (IDFs). Figure 6 shows a selection of FLN spectra of MPCl-DSPC at various excitation wavelengths. After the fitting procedure, the two most intensive peaks (characterized by ν_{vib1} = 1560 cm^{-1} and ν_{vib2} = 1230 cm^{-1}) were chosen for evaluation. We monitored the center of the actual peak (typical frequency ν_n) and the total area under the peak (proportional to the total emission intensity I_n), and determined the $\nu_n \rightarrow I_n$ functions. These functions change in accordance with the IDF (see eq App4). The difference in relative scale between the two series is a consequence of different intensities of spectral lines arising from the different absorption transition probabilities. Their relative value was estimated by the total relative area of the corresponding series, and their inverse was used as a weighting factor for normalization.

dx.doi.org/10.1021/jp304712n | J. Phys. Chem. B 2012, 116, 9644−9652

Table 1. Binding Parameters: n (Number of the Possible Binding Sites per Lipid Molecule), K_d (Dissociation Constant), $n/K_d = K_b$ (Binding Constant)

	DMPC [14]		DPPC [16]		DSPC [18]	
	MPE	MPCl	MPE	MPCl	MPE	MPCl
n	0.0083 ± 0.0026	0.0037 ± 0.0012	0.0044 ± 0.0008	0.0026 ± 0.0005	0.0079 ± 0.0013	0.0038 ± 0.0006
K_d (nM)	30 ± 10	52 ± 16	28 ± 7	53 ± 13	33 ± 9	15 ± 4
K_b (M^{-1})	2.8×10^5	7.1×10^4	1.6×10^5	4.9×10^4	2.4×10^5	2.5×10^5

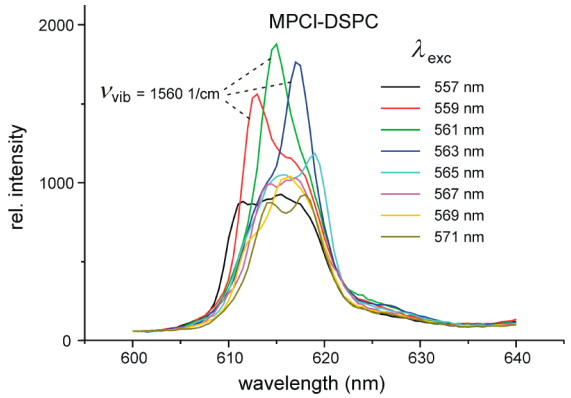

Figure 6. A series of fluorescence emission (line narrowing) spectra of MPCl-DSPC (SUV) in 50% (v/v) glycerol-PBS (pH 7.4) solution at 10 ± 1 K, excited at different wavelengths (λ_{exc}) marked by different colors. The shifts of the particular spectral peaks as a result of the change of the excitation wavelength are clearly visible. (The strongest spectral peak has a characteristic vibrational frequency (ν_{vib}) of 1560 cm^{-1}.)

Figure 7 shows the IDFs of MPCl incorporated in different SUVs prepared from different phosphatidylcholines in a standardized representation marked with symbols and the fitted black solid lines. The IDFs of MPE determined earlier are also presented by black broken lines for comparison.[19] According to the Gaussian decompositions of the IDFs, the bands identified earlier and here are denoted "site I–III" and marked by different colors: red, blue, and green, respectively. Fit results of the decomposition for both MPs are summarized in Table 2.

DISCUSSION

We applied fluorescence techniques to study the binding ability and location of two mesoporphyrin derivatives in liposomes. After the binding parameters (see Table 1) and the inhomogeneous distribution functions (IDFs) of both MPs incorporated in different SUVs (see Figure 7 and their parameters in Table 2) are determined, we compare and interpret the results.

Binding Ability. *MPE.* On the basis of the spectroscopic titrations, we showed that the two types of binding sites are totally equivalent in the case of DMPC samples, but in the two other cases (DPPC and especially DSPC), nonequivalent binding sites are present. The shape of the loops in Figure 3 shows the differences in binding parameters of the given samples. In this respect, the binding curve (see Figure 4) is much less sensitive. If the deviation of the two characteristic binding constants is less than 2 orders of magnitude, we cannot recognize any differences. Thus, the parameters of MPE binding in Table 1 are the mean values for the two types of sites.

As we can see in Table 1, the dissociation constants (K_d's) for MPE are practically identical (within error) in the case of all three samples differing in hydrocarbon chain lengths. Differences in the binding constants (K_b's) originate from the different n values, but the alteration is less than a factor of 2.

MPCl. We can observe that the dissociation constant is the same for DMPC and DPPC samples but much smaller for DSPC. Differences in binding constants are influenced by the n value as well; consequently, compared to MPE binding, we got 4 and 3 times smaller K_b values for DMPC and DPPC samples, respectively, but nearly the same for DSPC.

IDFs and Their Connection with the n Binding Parameter. In our earlier work,[19] we revealed some possible problems that may arise from the special technique of FLN, but we demonstrated that, due to glycerol addition and cryogenic cooling, liposomes are not destroyed but preserve their MP content. We also ruled out the notion that the IDF is caused by different aggregation states of MP associated with the liposomes.

The only open question in connection with the new samples is the protonation of the propionate groups. Since different protonation states may occur simultaneously in MPCl-SUV samples disturbing the interpretation of IDFs, we had to analyze this problem more carefully. On the basis of the results of simulation (Marvin Beans software), we found that all the possible groups are deprotonated in MPCl above pH 6. Since our measurements were done at pH 7.4, we may state that in our samples only the deprotonated form is present. Consequently, the possible components of the IDFs can be attributed to significantly different MP environments. These local environments can be identified as distinguishable locations in the liposome.

In Figure 7, it is visible at first sight that the two MPs have rather different IDFs in all three SUV samples. In Figure 7A, we can only see a single band characteristic of the DMPC-MPCl sample, while in Figure 7C one can observe the dual character of the IDF of DSPC-MPCl. Such a dual character is only hardly visible in the case of the DPPC-MPCl sample (Figure 7B).

We can also observe that all the samples, except for DMPC-MPCl, have a composite IDF providing evidence for the existence of more than one type of MP site. We may decompose the IDFs into Gaussian bands, parameters of which are shown in Table 2. The center is characteristic of the subpopulation of molecules, while the fwhh (full width of the band at half height) parameter measures the heterogeneity of its environment. The relative area under the band is proportional to the total amount of molecules associated with a certain site.

The fit parameters can be connected to "sites I, II, and III". We can see in Table 2 that "site II" can be found in the IDF of all samples. Though the heterogeneity of environment is different, the agreement between the centers for MPE and MPCl in any given SUV sample proves the identity of these sites. It is also observable that the earlier identified "site I"

dx.doi.org/10.1021/jp304712n | J. Phys. Chem. B 2012, 116, 9644–9652

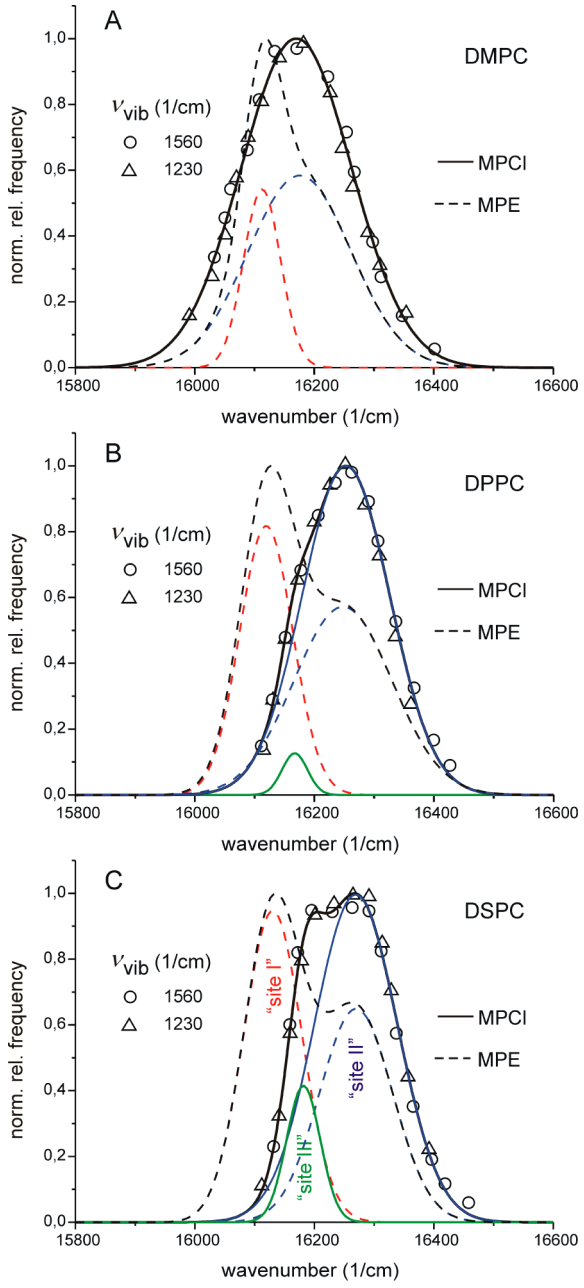

Figure 7. Inhomogeneous distribution functions (IDFs) (with their Gaussian decompositions) of the two MPs incorporated in different SUVs prepared from different phosphatidylcholines (in a standardized representation). The broken and solid lines indicate MPE and MPCl, respectively. The SUVs are composed of either DMPC (A), DPPC (B), or DSPC (C). In the case of MPCl samples, IDFs were prepared by using two dominant spectral peaks marked with different symbols according to the characteristic vibrational frequency (○, 1560 cm^{-1}; Δ, 1230 cm^{-1}; the stronger one is clearly seen in Figure 6). According to the Gaussian decompositions, in part C, we marked the bands as "site I" (red), "site II" (blue), and "site III" (green). (Standard errors are comparable to the symbol size.)

disappeared from all the IDFs of MPCl samples, and a new one named "site III" appeared in the case of DPPC and DSPC samples.

We thought that as a consequence of these changes we can find a relation between the n values (see Table 1) of the various samples. Let us consider the DPPC and DSPC samples. (The DMPC sample has much less confidence for such calculations due to the structural sensitivity caused by the considerably lower main transition temperature T_m.) Since "site I" does not exist in the IDFs of MPCl samples, the number of the possible binding sites n should decrease compared to the MPE samples by a factor, which is given as a fraction of molecules associated with "site II". From Table 2, we can read these values: 0.56 for DPPC and 0.46 for DSPC. Let us multiply the n values of MPE-SUV samples (0.0044 and 0.0079, see Table 1) by these factors; the results are 0.0025 and 0.0036, respectively. If we compare these numbers with 0.0026 and 0.0038 found in Table 1 for MPCl-SUV samples, and take into consideration the presence of the "site III" population in these samples as well as the considerable errors, the agreement is rather good.

Interpretation of MP Association at Molecular Level. Using some geometrical parameters of the SUV, the number of lipid molecules per liposome (N_{tot}) can be estimated by the following formula (Encapsula NanoSciences, Nashville, TN):

$$N_{tot} = \frac{4\pi\left(\frac{d}{2}\right)^2 + 4\pi\left(\frac{d}{2} - h\right)}{a} \quad (4)$$

where d is the liposome diameter, h is the bilayer thickness, and a is the headgroup area. In our case, $N_{tot} \approx 10^4$ for a DPPC-SUV sample ($d \approx 38$ nm, $h \approx 5$ nm, $a \approx 0.7$ nm^2). On the basis of this information, we determined that the actual concentration of liposomes in their suspensions is about 700 nM and the local concentration of mesoporphyrin in the liposomes is ≈30/pieces. These data are characteristic of the system from different aspects and reveal a number of connections between the macroscopic and microscopic levels.

The main question is how to identify the "sites" of MP found in IDFs with the locations in the SUVs. In some earlier works, the location of a photosensitizer in the bilayer was characterized by the depth which can uniquely determine the location, and the dye molecules were assumed to remain more or less parallel to the hydrocarbon chains.[13,15,17,18,27,28] There are some other concepts of the location of small molecules within the liposomal bilayer (e.g., they are actually sandwiched between the layers, i.e., at the end of the fatty acid chains).[29−31]

We have previously proposed a model for MPE-SUV samples where "site I" corresponds to locations between the two lipid layers ("perpendicular sites") and "site II" to locations along the hydrocarbon chains ("parallel sites").[19] On the basis of this model, we could explain the changes of IDFs as a result of the changing length of hydrocarbon chains in the different SUVs.

Here we show that our model is also suitable (with minor supplementations) for the identification of "sites" in the MPCl-SUV samples. On the basis of the simulation (Marvin Beans software), we can compare the hydrophilic and hydrophobic properties of the two mesoporphyrin derivatives. While MPE has no charges at pH 7.4, MPCl has two negative charges due to the deprotonation of the propionate groups; therefore, the MPCl molecule is less hydrophobic than its esterified form. This fact provides an explanation for the disappearance of "site I" ("perpendicular sites") from the IDFs of all MPCl-SUVs because the MPCl molecule cannot be located in the extraordinarily hydrophobic environment between the two lipid layers.

It has been shown earlier that the protoporphyrin is deeply buried in the hydrocarbon regions of the membrane.[11] The parallax method enables the determination of the depth of a fluorophore in a membrane bilayer along the hydrocarbon

dx.doi.org/10.1021/jp304712n | J. Phys. Chem. B 2012, 116, 9644−9652

Table 2. Parameters of the IDFs Fitted by Gaussians: Center, fwhh (Full Width of the Band at Half Height), Relative Area

		DMPC [14]		DPPC [16]		DSPC [18]	
		MPE	MPCl	MPE	MPCl	MPE	MPCl
"site I"	center (1/cm)	16112 ± 1	not present	16119 ± 2	not present	16130 ± 3	not present
	fwhh (1/cm)	73 ± 6		104 ± 5		115 ± 6	
	rel. area	0.25		0.44		0.54	
"site II"	center (1/cm)	16175 ± 6	16176 ± 1	16248 ± 9	16257 ± 4	16270 ± 6	16268 ± 7
	fwhh (1/cm)	203 ± 7	186 ± 2	194 ± 14	151 ± 5	144 ± 11	137 ± 9
	rel. area	0.75	1.0	0.56	0.95	0.46	0.85
"site III"	center (1/cm)	not present	not present	not present	16177 ± 5	not present	16181 ± 3
	fwhh (1/cm)				55 ± 11		55 ± 9
	rel. area				0.05		0.15

chains by the relative quenching that is observed with different membrane-bound quenchers whose own depth is known.[18] The distance of the protoporphyrin from the center of the bilayer obtained by this method in DMPC-SUV is less than 1 nm. Compared to the total width of the bilayer, which is about 4.5 nm, we may confirm that this molecule can be found indeed in the hydrocarbon regions of the membrane. Since proto- and mesporphyrin (MPCl) are rather similar molecules with respect to their lipophilicity parameters and the partitioning into membranes,[32] we may conclude that the preferred region of the MPCl is also the deeper part of the membrane along the hydrocarbon chains.

The "site II" component of the IDFs of the MPE-SUV samples was identified earlier as the "parallel sites" described above. Since the respective center parameters of "site II" are practically identical for MPE and MPCl (see Table 2), it provides evidence of the presence of the "parallel sites" in MPCl-SUV samples as well. Decrease of the fwhh parameters of "site II" in MPCl-SUV compared to MPE-SUVs at each chain length can be explained by the higher order of the hydrocarbon chains due to the absence of "perpendicular sites".

According to our proposal, "site III" corresponds to MPs located along the outer part of the hydrocarbon chains partially inserted between the lipid head groups. Thus, we can distinguish two types of "parallel sites" in MPCl-SUV samples forming two MP subpopulations, namely, the inner "site II" and the outer "site III". This concept can be supported by the following arguments.

It is well-known that below the pretransition temperature (T_p), which is ≈15, 35, and 51 °C for our respective SUV samples with increasing chain length, the head groups of membrane lipids also have an ordered structure, which is not independent of the order of the hydrocarbon chains.[33,34] Since our measurements were performed at room temperature (RT ≈ 22 °C), the head groups in the samples must be in the ordered phase except for DMPC-SUV, giving a plausible explanation for the absence of "site III" in the IDF of MPCl-DMPC. The center and fwhh parameters of the "site III" band of the other two samples (DPPC and DSPC) are almost identical and the distribution is rather narrow, confirming the existence of a well-defined location.

The only remarkable difference between the two samples derives from the different thickness of the bilayers. As we learned above, the preferred region of MPCl is the deeper, rather hydrophobic part of the membrane along the hydrocarbon chains. If the bilayer is thick enough, molecules can be totally immersed into the hydrophobic region and fill the available space, forming the "inner parallel sites". However, the limited thickness of the bilayer may confine the formation of "outer parallel sites": the narrower the bilayer, the fewer the space for formation of new binding sites, explaining the varying amount of molecules associated with the "outer parallel site" in samples of different chain legths, resulting in varying values for the relative area under the "site III" band in the IDFs (see Table 2).

We suppose that the increased binding constant of the MPCl-DSPC sample is at least in part a consequence of the presence of the "outer parallel sites". As we mentioned, the obtained binding constant is the common weighted average of the individual binding constants of the inner and outer "parallel sites"; the weights depend on the amount of assotiated MPs. We propose that the increase can be attributed to the binding constant of the outer "parallel sites", while that of the inner one remains relatively constant. While in the MPCl-DMPC sample "outer parallel sites" are not present at all, in the MPCl-DPPC, its contribution seems to be negligible, leaving the K_d parameter unchanged, but in the MPCl-DSPC, its presence is definitive decreasing the K_d parameter by a factor of 3.5.

CONCLUSIONS

We provided answers to some long-standing questions in connection with the binding ability and location of photosensitizers in liposomes. We used MPE and MPCl as sensitizers associated with monocomponent SUVs formed by DMPC, DPPC, and DSPC, as simple models of a cellular membrane, and the methods of conventional and site-selective fluorescence spectroscopy were applied. We determined the IDFs of both MPs in different liposome environments and pointed to the presence of two well-defined populations and corresponding locations for each MP. We also determined the binding parameters, which can be considered as the means of the values concerning the corresponding sites. We could show the existence of nonequivalent binding sites in cases when it was not obvious at all. We found in general that the binding ability of MPE is considerably greater than that of MPCl. The exception (MPCl-DSPC sample) is a consequence of the newly identified locations. On the basis of the fit results of the decomposition of the IDFs into Gaussians, we proposed a consistent interpretation of our results at the molecular level, providing new evidence for our extended earlier model. Namely, one of the locations (for MPE) is between the two lipid layers, another one (for MPE and MPCl) is located deeply between the hydrocarbon chains, and a third one (for MPCl) is along the outer part of the hydrocarbon chains partially inserted between the head groups of lipid molecules. Existence of the binding location between the two lipid layers for MPE, which is inaccessible for MPCl, and the higher binding ability of MPE provide relevant information regarding the practical application

dx.doi.org/10.1021/jp304712n | J. Phys. Chem. B 2012, 116, 9644−9652

of the esterified derivatives of mesoporphyrins as photosensitizers.[35]

APPENDIX I

The basic principles of the FLN technique are the following. Fluorescence emission spectra are measured on samples that are rapidly cooled from room temperature to cryogenic temperatures. As a consequence of the cooling, the atomic configurations surrounding the chromophore that are populated at room temperature become fixed. This conserved population can be studied by spectroscopy. The term "site" in the name of the technique means a molecular environment of the dye molecule as well as the corresponding detuned electronic transition energy of the dye molecule in this specific environment. With the use of narrow bandwidth ($\Delta\nu$) excitation, only part of the molecules is selectively excited. This subpopulation of the chromophores represents a set of specific frozen environments. Because of the selective excitation, the emission spectra consist of sharp emission lines resulting from resonant excitations superimposed on the background of broad bands, which are present due to the nonresonant excitation. The mth line originates from the transition between the lowest vibrational level of the first electronic excited state (1, 0) and the ground state (0, 0) after an excitation of (1, m) ← (0, 0) and a vibrational relaxation (1, m) → (1, 0). In a background-subtracted spectrum, the line intensity (I_m) is given by

$$I_m = KI_{exc}AB_mN_m(\nu, \Delta\nu) \quad \text{(App1)}$$

where K is a constant, I_{exc} is the excitation intensity, A is the fluorescence emission probability, B_m is the absorption transition probability, and $N_m(\nu, \Delta\nu)$ denotes the number of selectively excited molecules at a given excitation frequency (ν) and excitation bandwidth ($\Delta\nu$).[36] In most cases, $N_m(\nu, \Delta\nu)$ can be given as

$$N_m(\nu, \Delta\nu) = N_0\left[n_m\left(\nu + \frac{\Delta\nu}{2}\right) - n_m\left(\nu - \frac{\Delta\nu}{2}\right)\right] \quad \text{(App2)}$$

where N_0 is the total number of the excitable dye molecules and $n_m(\nu)$ is their cumulative distribution function (CDF_m) characteristic for the inhomogeneous broadening, which has a same common shape for all the spectral lines (m = 0, 1, 2, ...) shifted along the frequency scale. Instead of CDF_m, we may use the spectral density function (SDF_m) or $n_m'(\nu)$ which is the derivative of $n_m(\nu)$:

$$N_m(\nu, \Delta\nu) = N_0n_m'(\nu)\Delta\nu \quad \text{(App3)}$$

Let us choose the $n_0'(\nu)$ function which is a possible representation of the so-called inhomogeneous distribution function (IDF ≡ SDF_0 in this paper). Since the source of the inhomogeneous broadening is the varying chromophore environment, this function is characteristic for the site distribution of chromophore molecules in their environments.

For high selectivity, a high-resolution luminometer with narrow bandwidth on the excitation and the emission sides is required. We have shown that we do not need to use extreme high resolution if the IDF consists of moderately sharp bands ("moderate site-selectivity").[19] In a lower-resolution spectrum, instead of double lines or line groups, only broader envelopes as "virtual" lines or peaks are observed. Equations App1−App3 remain valid for these peaks (I_n) because of the additive nature of light intensity:

$$I_n = KI_{exc}AB_nN_0n_n'(\nu)\Delta\nu \quad \text{(App4)}$$

If we record fluorescence emission spectra at several excitation wavelengths, these peaks will shift according to the change of the excitation wavelength because the difference between the nth peak frequency and the actual excitation frequency results in a typical vibrational frequency ($\nu_n - \nu_{exc} = \nu_{vib,n}$) characteristic of the nth peak itself. The relative intensity of such a peak will change in accordance with the IDF (more precisely, with the $n_n'(\nu)$), and the differences between the peaks arising from the different absorption transition probabilities are taken into consideration by the B_n parameter. All the other parameters in eq App4 remain constant. Since background correction becomes simpler and less ambiguous, and the larger signal results in an improved signal-to-noise ratio, this method does not provide a less reliable IDF than the higher resolution technique.[19]

APPENDIX II

Because the free MPE is nonfluorescent, the measured fluorescence intensity I is proportional to the $[MP]_b$. If the binding sites are equivalent or indistinguishable in the association process, the proportionality is valid at each wavelength:

$$I(\lambda) = m(\lambda)[MP]_b \quad \text{(App5)}$$

where $m(\lambda)$ is independent of lipid concentration and characteristic only of the shape of the spectra. Let us consider

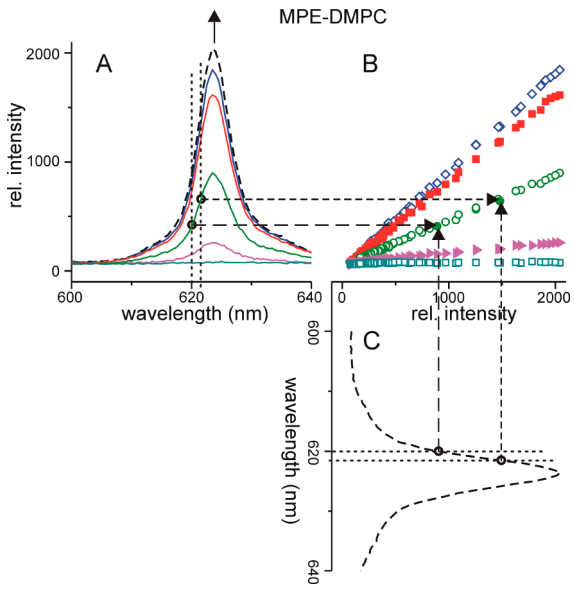

Figure 8. Principles of a novel representation for the evaluation process of MPE binding to SUVs. (A) Spectroscopic titration of MPE-DMPC as seen in Figure 1. (C) The same kind of spectrum at maximum lipid concentration ([L]max) rotated 90° clockwise. (B) The $I_{[L]max}(\lambda) \rightarrow I_{[L]}(\lambda)$ functions at a series of lipid concentrations; these are derived from relative intensity values corresponding to simultaneously changing wavelengths (see text). For a better understanding, the mapping of the green curve at 620 and 621.5 nm is indicated by arrows with longer and shorter broken lines, respectively.

dx.doi.org/10.1021/jp304712n | J. Phys. Chem. B 2012, 116, 9644−9652

two spectra at different lipid concentrations, [L]1 and [L]2, respectively. According to eq App5:

$$I_{[L]1}(\lambda) = I_{[L]2}(\lambda)\frac{m(\lambda)[MP_1]_b}{m(\lambda)[MP_2]_b} = k_{1,2}I_{[L]2}(\lambda) \quad \text{(App6)}$$

where the $[MP_1]_b/[MP_2]_b$ ratio is noted by $k_{1,2}$. If we use the maximum concentration of lipid ([L]max) as a reference value and take into consideration the background correction, we may generalize eq App6:

$$I_{[L]}(\lambda) = k_{[L]}I_{[L]max}(\lambda) + C \quad \text{(App7)}$$

where the slope, $k_{[L]}$, gives the relative $[MP]_b$ (to the $[MP]_b$ at the maximum concentration of lipid) and C is a constant. Thus, if we represent the $I(\lambda)$ values as a function of $I_{[L]max}(\lambda)$ values according to the simultaneously changing wavelength ($I_{[L]max}(\lambda) \rightarrow I_{[L]}(\lambda)$ but not as a function of λ), we get a straight line with a slope of $k_{[L]}$.

Figure 8 shows the basic principles of this representation. In Figure 8A, we can see a series of conventional fluorescence emission spectra of the MPE-DMPC at constant MP and various lipid concentrations. In Figure 8C, the highest component (with maximum lipid concentration) of the previous series after a 90° clockwise rotation is visible. Figure 8B shows the final result of this procedure, namely, the $I_{[L]max}(\lambda) \rightarrow I_{[L]}(\lambda)$ functions.

AUTHOR INFORMATION

Corresponding Author

*Phone/Fax: 36-1-266-6656. E-mail: herenyi.levente@med.semmelweis-univ.hu.

Notes

The authors declare no competing financial interest.

ACKNOWLEDGMENTS

We are very grateful to Gergely Gyimesi for helpful discussions and to Prof. Miklós Kellermayer, Katalin Kis-Petik, and Gergely Agócs for the careful reading of the manuscript. This work was supported by Hungarian grants: TÁMOP-4.2.1/B-09/1/KMR-2010-0001, TÁMOP-4.2.2/B-10/1-2010-0013, OTKA K-84271, and OMFB-380/2007.

REFERENCES

(1) Brown, S. B.; Brown, E. A.; Walker, I. *Lancet Oncol.* **2004**, *5*, 497−508.
(2) Nyman, E. S.; Hynninen, P. H. *J. Photochem. Photobiol., B* **2004**, *73*, 1−28.
(3) Dougherty, T. J. *Photomed. Laser Surg.* **2002**, *20*, 3−7.
(4) Qiang, Y. G.; Zhang, X. P.; Li, J.; Huang, Z. *Chin. Med. J.* **2006**, *119*, 845−857.
(5) Ben-Hur, E.; Geacintov, N. E.; Studamire, B.; Kenney, M. E.; Horowitz, B. *Photochem. Photobiol.* **1995**, *61*, 190−195.
(6) Wainwright, M. *Photochem. Photobiol. Sci.* **2004**, *3*, 406−411.
(7) Jori, G.; Brown, S. B. *Photochem. Photobiol. Sci.* **2004**, *3*, 403−405.
(8) Dror, S. B.; Bronshtein, I.; Garini, Y.; O'Neal, W. G.; Jacobi, P. A.; Ehrenberg, B. *Photochem. Photobiol. Sci.* **2009**, *8*, 354−361.
(9) Ytzhak, S.; Bernstein, S.; Loew, L. M.; Ehrenberg., B. *Proc. Soc. Photo-Opt. Instrum. Eng.* **2009**, *7380*, 7380291−10.
(10) Lang, K.; Mosinger, J.; Wagnerová, D. M. *Coord. Chem. Rev.* **2004**, *248*, 321−350.
(11) Ricchelli, F. *J. Photochem. Photobiol., B* **1995**, *29*, 109−118.
(12) Hoebeke, M. *J. Photochem. Photobiol., B* **1995**, *28*, 189−196.
(13) Angeli, N. G.; Lagorio, M. G.; San Román, E. A.; Dicelio, L. E. *Photochem. Photobiol.* **2000**, *72*, 49−56.
(14) Postigo, F.; Mora, M.; De Madariaga, M. A.; Nonell, S.; Sagristá, M. L. *Int. J. Pharm.* **2004**, *278*, 239−254.
(15) Ricchelli, F.; Jori, G. *Photochem. Photobiol.* **1986**, *44*, 151−157.
(16) Ricchelli, F.; Jori, G.; Gobbo, S.; Tronchin, M. *Biochim. Biophys. Acta* **1991**, *1065*, 42−48.
(17) Lavi, A.; Weitman, H.; Holmes, R. T.; Smith, K. M.; Ehrenberg, B. *Biophys. J.* **2002**, *82*, 2101−2110.
(18) Bronshtein, I.; Afri, M.; Weitman, H.; Frimer, A. A.; Smith, K. M.; Ehrenberg, B. *Biophys. J.* **2004**, *87*, 1155−1164.
(19) Herenyi, L.; Veres, D.; Békási, S.; Voszka, I.; Módos, K.; Csík, G.; Kaposi, A. D.; Fidy, J. *J. Phys. Chem. B* **2009**, *113*, 7716−7724.
(20) Personov, R. I. In *Spectroscopy and excitation dynamics of condensed molecular systems*; Agranovich, V. M., Hochstrasser, R. M., Eds.; North-Holland: Amsterdam, The Netherlands, 1983; Chapter 10.
(21) Avarmaa, R. A.; Rebane, K. K. *Spectrochim. Acta* **1985**, *41A*, 1365−1380.
(22) Personov, R. I. *J. Photchem. Photobiol., A* **1992**, *62*, 321−332.
(23) Bryan, R. K. In *Maximum Entropy and Bayesian Methods*; Fougere, P. F., Ed.; Kluwer Academic: Dordrecht, The Netherlands/Norwell, MA, 1990; pp 221−232.
(24) Modos, K.; Galantai, R.; Bardos-Nagy, I.; Waschmuth, M.; Toth, K.; Fidy, J.; Langowski, J. *Eur. Biophys. J.* **2004**, *33*, 59−67.
(25) Zierler, K. *Biophys. Struct. Mech.* **1977**, *3*, 275−289.
(26) Bashford, C. L.; Smith, J. C. *Biophys. J.* **1997**, *25*, 81−85.
(27) Ricchelli, F.; Gobbo, S. *J. Photochem. Photobiol., B* **1995**, *29*, 65−70.
(28) Gross, E.; Ehrenberg, B. *Biochim. Biophys. Acta* **1989**, *983*, 118−122.
(29) White, S. H.; King, G. I.; Cain, J. E. *Nature* **1981**, *290*, 161−163.
(30) Katsikas, H.; Quinn, P. J. *FEBS Lett.* **1981**, *133*, 230−234.
(31) Afri, M.; Ehrenberg, B.; Talmon, Y.; Schmidt, J.; Cohena, Y.; Frimer, A. A. *Chem. Phys. Lipids* **2004**, *131*, 107−121.
(32) Kępczyński, M.; Pandian, R. P.; Smith, K. M.; Ehrenberg, B. *Photochem. Photobiol.* **2002**, *76*, 127−134.
(33) O'Leary, T. J.; Ross, P. D.; Levin, I. W. *Biophys. J.* **1986**, *50*, 1053−1059.
(34) Riske, K. A.; Barroso, R. P.; Vequi-Suplicy, C. C.; Germano, R.; Henriques, V. B.; Lamy, M. T. *Biochim. Biophys. Acta* **2009**, *1788*, 954−963.
(35) Krammer, B.; Verwanger, T. *Med. Laser Appl.* **2009**, *24*, 221−226.
(36) Herenyi, L.; Suisalu, A.; Mauring, K.; Kis-Petik, K.; Fidy, J.; Kikas, J. *J. Phys. Chem. B* **1998**, *102*, 5932−5940.